Supporting Information

Culurgioni et al. 10.1073/pnas.1113077108

SI Materials and Methods

Protein Preparation. GST-Pins$^{25–444}$:Insc$^{252–263}$ was purified by affinity and anion-exchange. All Pins and LGN mutants were purified similarly. Human NuMA$^{1,807–1,987}$ was purified by nickel affinity and cation-exchange. To map the minimal interacting regions, Pins$^{25–444}$:Insc$^{252–263}$ was incubated with trypsin in a 30:1 wt:wt ratio for 1 h at 4 °C, and analyzed by ESI-MS (ProMiFa). Human LGN:Gαi^{GDP} was produced from insect cells by colysis with Gαi$^{26–354}$, and purified as reported (1). Human Insc:LGN:Gαi^{GDP} complex was generated by coinfection with two baculoviruses. For crystallization studies, the proteolyzed Pins$^{25–406}$:Insc$^{303–340}$ was concentrated up to 10 mg/mL in 10 mM Hepes pH 7.5, 0.1 M NaCl and 1 mM DTT.

Crystallization and Crystal Structure Determination. Pins$^{25–406}$:Insc$^{303–340}$ was crystallized by hanging-drop vapor diffusion at 20 °C with a reservoir containing 0.1 M Tris-HCl pH 8.5, 0.2 M Magnesium chloride hexahydrate and 15% PEG 4000. For data collection, crystals were transferred to a cryo buffer (reservoir buffer supplemented with 20% ethylene glycol), and flash-frozen in liquid nitrogen. Crystallization experiments were performed at the Crystallography Unit of the IFOM-IEO Campus (Milan). X-ray diffraction data were collected at beamline ID23-1 at European Synchrotron Radiation Facility (Grenoble). Data were processed with HKL2000 (2). Initial phases were derived using SHELX in hkl2map (3). Model building was initiated with helical fragments placed into the electron density by Phenix (4), and completed using iterative cycles of manual model building in COOT (5) and restrained refinement. The final model contains residues 39–386 of Pins^{TPR}, and residues 307 to 335 of dInsc^{PEPT}. The loop 369–374 of Pins^{TPR} connecting the αB8 helix of the last TPR with the capping helix αC is missing as the density in this region is rather poor. For analogous reasons, only a poly-Ala model could be built for the terminal αC helix. Data statistics are shown in Table S1.

In Vitro Binding Assays. To test the effect of point mutations, GST-dInsc$^{303–340}$, GST-hInsc$^{24–58}$, and GST-NuMA$^{1,886–1,914}$ (0.2 μM) adsorbed on GSH-beads were incubated for 1 h at 4 °C with 0.2–0.4 μM of the chosen TPR construct in a buffer containing 10 mM Hepes pH 7.5, 0.1 M NaCl, 5% glycerol, 0,1% Triton X-100, 0,1% Tween20 and 0,1% Na-deoxycholate.

ITC. Lyophilized dInsc$^{303–340}$, hInsc$^{24–58}$, and NuMA$^{1,886–1,914}$ peptides and TPR domains were dialyzed against 10 mM Hepes pH 7.5, 0.15 M NaCl and 5% glycerol. ITC measurements were performed on a MicroCal VP-ITC (MicroCal, Inc).

Fluorescence Polarization. Fluorescence polarization measurements were performed on an Infinite F200 (Tecan). Fluorescein-labeled NuMA^{PEPT} (15 nM) was incubated with 250 nM LGN^{TPR} in the presence of increasing concentration of unlabeled hInsc^{PEPT} in 10 mM Hepes pH 7.5, 0.15 M NaCl, 0.5 mM EDTA and 1 mM DTT. A similar experiment was performed titrating unlabeled NuMA^{PEPT} into a mixture of fluorescein-hInsc^{PEPT}.

1. Tall GG, Gilman AG (2005) Resistance to inhibitors of cholinesterase 8A catalyzes release of Galphai-GTP and nuclear mitotic apparatus protein (NuMA) from NuMA/LGN/Galphai-GDP complexes. *Proc Natl Acad Sci USA* 102:16584–16589.
2. Minor ZOaW (1997) Processing of X-ray diffraction data collected in oscillation mode. *Methods in Enzymology* Volume 276:307–326.
3. Pape T, Schneider TR (2004) HKL2MAP: a graphical user interface for phasing with SHELX programs. *J Appl Cryst* 37:843–844.
4. Adams PD, Grosse-Kunstleve RW, Hung LW, Ioerger TR, McCoy AJ, Moriarty NW, Read RJ, Sacchettini JC, Sauter NK, Terwilliger TC (2002) PHENIX: building new software for automated crystallographic structure determination. *Acta Crystallogr D Biol Crystallogr* 58:1948–1954.
5. Emsley P, Cowtan K (2004) COOT: Model-building tools for molecular graphics. *Acta Cryst* D60:2126–2132.

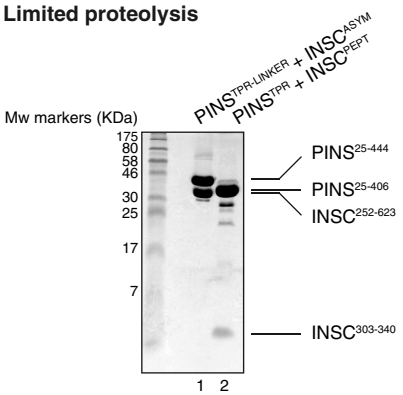

Fig. S1. SDS-PAGE of the untreated and trypsinized sample that was submitted to Mass Spectrometry analysis.

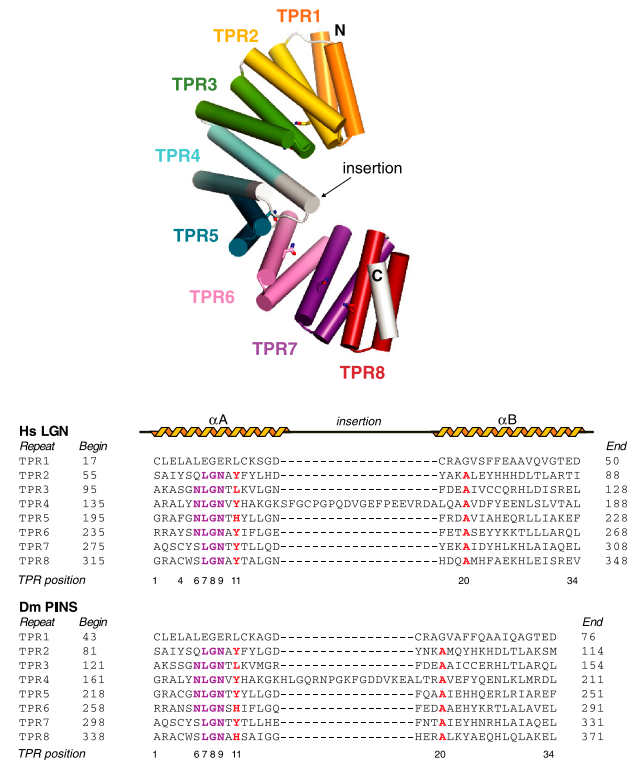

Fig. S2. Top: cartoon drawing of the Pins^{TPR} architecture showing the TPRs. Invariant Asn are shown in sticks. Bottom: alignment of the TPR motifs of LGN and Pins. The structure-based alignment of TPR sequences of LGN and Pins highlights the presence of NLGN motifs in the αA helix (in purple), and of conserved hydrophobic residues (in red) conforming to the canonical TPR consensus (shown at the bottom). The presence of a 17-20 residues insertion between helix αA and αB of TPR4 is visible in both proteins.

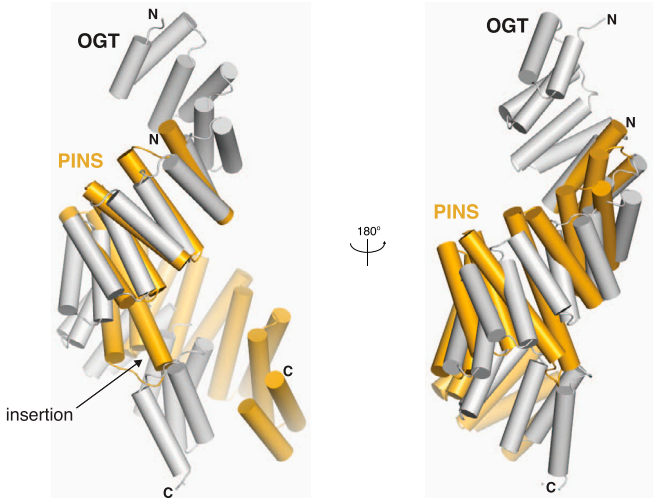

Fig. S3. Structural comparison of Pins^{TPR} and OGT. The topological features of the Pins^{TPR} superhelical arrangements were compared with OGT using the server Rapido, which revealed the presence of an invariant rigid body consisting of the first TPR of Pins^{TPR} (residues 42 to 70) and the third TPR of OGT (residues 112 to 140). Superposition of Pins^{TPR} (in gold) and OGT (in light gray) on this rigid body shows an outward displacement of the helical axis of Pins^{TPR} caused by the TPR4 insertion, which would otherwise clash on the following helical turn. Two orthogonal views are shown.

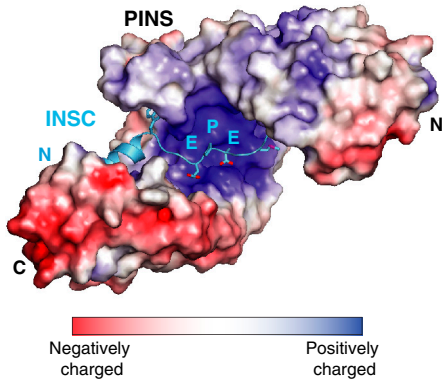

Fig. S4. Surface views of Pins^{TPR} colored by electrostatic potential. The EPE^{Insc} triplet is shown in sticks.

Fig. S5. Sequence alignment of Insc orthologs. Insc residues are colored according to their conservation, which was calculated based on alignment of five orthologs from *Drosophila melanogaster*, *Homo sapiens*, *Mus musculus*, *Gallus gallus* and *Oryzias latipes* (*Medaka*). The secondary structure of the region corresponding to dInsc^{PEPT} as derived from structural analysis is displayed on top of the alignment, with the residues required for the interaction with Pins^{TPR} indicated by red circles. Purple triangles mark the boundaries of the *Drosophila* asymmetric domain.

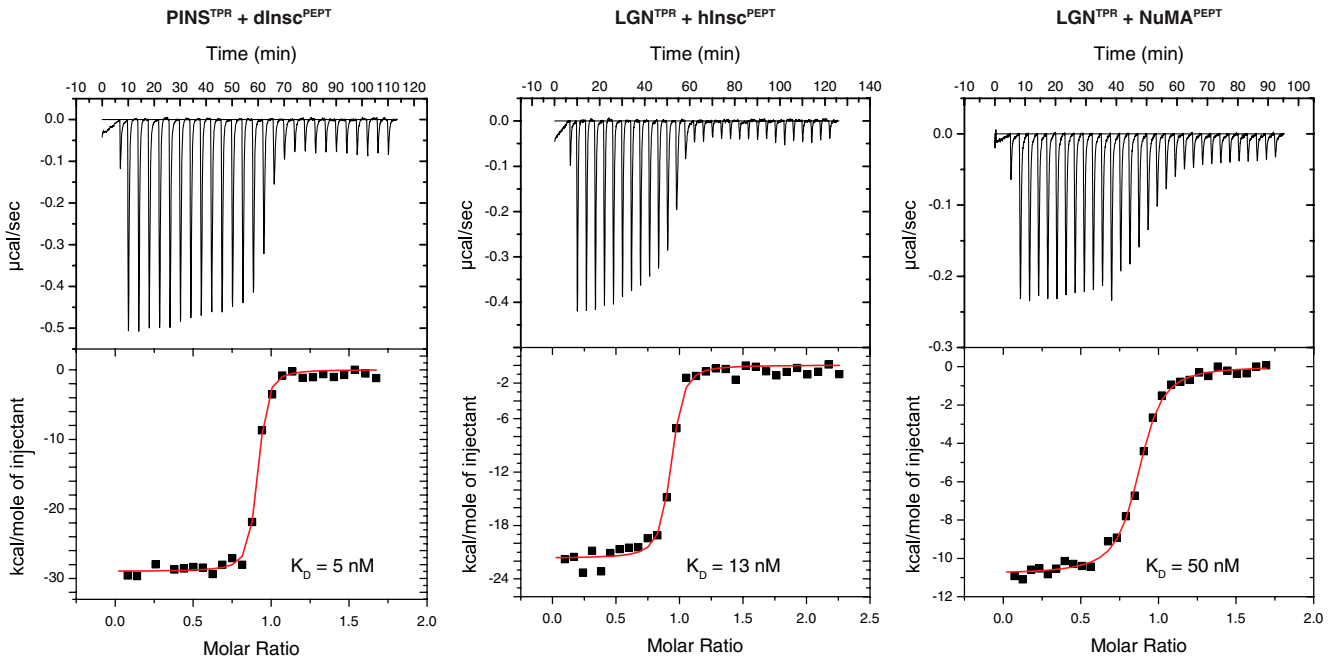

Fig. S6. Measurement of binding affinities between Pins^{TPR}:dInsc^{PEPT}, LGN^{TPR}:hInsc^{PEPT}, and LGN^{TPR}:NuMA^{PEPT}. Isothermal Titration Calorimetry experiments revealed that Pins^{TPR} binds dInsc^{PEPT} with an affinity comparable to the one of LGN^{TPR} for hInsc^{PEPT}, with dissociation constants of 5 nM and 13 nM respectively. NuMA^{PEPT} binds LGN^{TPR} with a lower affinity, with a K_D of 50 nM. All reactions are exothermic and exhibit a 1:1 stoichiometry.

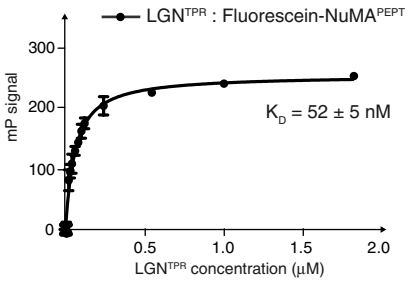

Fig. S7 Fluorescence polarization measurement of the binding affinity between LGN^{TPR} and NuMA^{PEPT}. LGN^{TPR} was titrated into 15 nM of fluorescein-labeled NuMA$^{1886–1914}$. Fitting of the polarization curve yielded a dissociation constant of 52 nM, in agreement with the value obtained for the same reaction by ITC (Fig S6). The experiment established conditions for the fluorescence polarization-based competition assays presented in Fig. 4*C*.

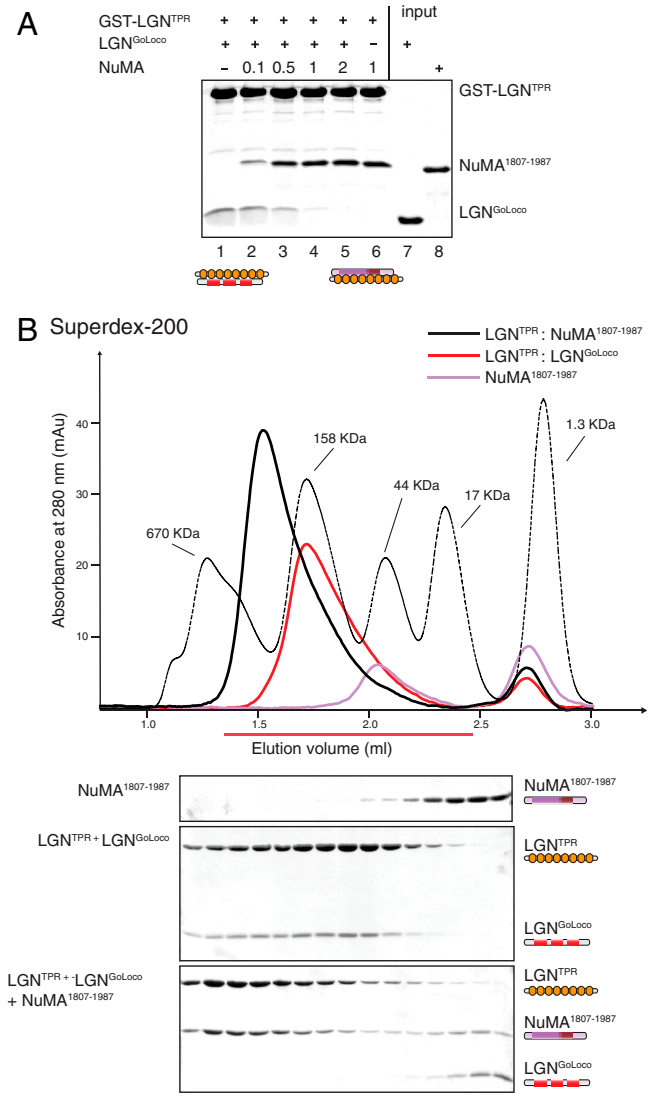

Fig. S8 NuMA disrupts the LGN^{TPR}:LGN^{GoLoco} interaction. (*A*) A GST-LGN^{TPR} fusion protein (2 μM) was adsorbed on GSH beads, and its ability to interact with LGN^{GoLoco} was analyzed in the presence of increasing amounts of NuMA$^{1821–2001}$. Upon addition of NuMA$^{1807–1987}$ the retention of LGN^{GoLoco} on beads was proportionally reduced confirming that NuMA competes for the binding to LGN^{TPR}. Already at roughly equimolar NuMA$^{1807–1987}$ and LGN^{GoLoco} concentrations, NuMA$^{1807–1987}$ remained bound to LGN^{TPR}, indicating that it is a higher-affinity ligand, whose binding interferes with the closed state of LGN. (*B*) The ability of NuMA to open the LGN switch was tested by size exclusion chromatography (SEC). Upon NuMA$^{1807–1987}$ addition, LGN^{GoLoco} is displaced from LGN^{TPR}.

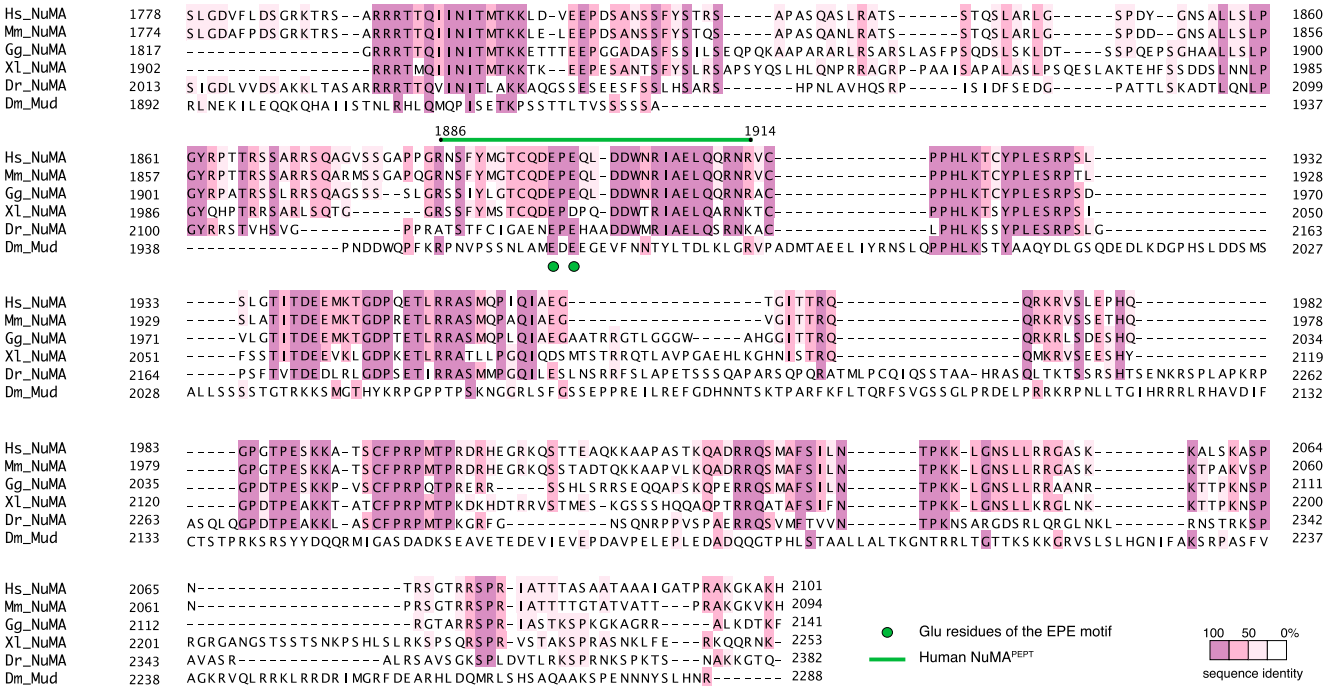

Fig. S9 Sequence alignment of the C-terminal portion of NuMA orthologs. Coloring of NuMA reflects the conservation among homologues from *Homo sapiens*, *Mus musculus*, *Gallus gallus*, *Xenopus laevis*, *Danio rerio*, and *Drosophila melanogaster*. The sequence of human NuMA^{PEPT} encompassing the LGN^{TPR} binding site is indicated in green on top of the alignment, with the invariant glutamic acid residues of the EPE motif marked as green circles. *Drosophila* Mud shares little sequence similarity with the other NuMA orthologs even in the Pins-binding region, where consecutive EPE-EGE triplets are present.

Table S1. Data Collection and Refinement Statistics

Data set	Pins-Insc native	Pins-Insc SeMet SAD
Beamline	ESRF ID23-1	ESRF ID23-1
Space group	C2	C2
Wavelength (Å)	0.979	0.979
Unit cell dimensions (Å)	160.2	159.29
	64.23	64.20
	107.60	107.20
	$\beta = 117.9°$	$\beta = 118.2°$
Resolution (Å) *	25.0–2.1 (2.18–2.1)	20.0–3.0 (3.1–3.0)
Total observations	472,231	733,917
Unique reflections	56,295	19,213
Data completeness (%)	98.7 (96.7)	99.8 (98.9)
Rsym (%) †	5.6 (22.4)	11.4 (29.9)
$I/\sigma I$	12.5 (2.3)	11.4 (3.5)
Refinement		
Resolution range (Å)	23.5–2.1	
Rwork / Rfree †	20.8/25.6	
Number of protein atoms	5,755	
Number of solvent atoms	487	
rmsd bond lengths (Å)	0.019	
rmsd bond angles (°)	1.59	
Mean B-factor protein (Å^2)	42.1	
Ramachandran values		
Favored (%)	98.1	
Allowed (%)	1.9	
Outliers (%)	0	

*Values in parentheses refer to the outer resolution shell.

†R_{free} is equivalent to R_{conv} for a 5% subset of reflections not used in the refinement.